

A Block Least Mean Square Method for Fiber Longitudinal Power Profile Monitoring

Paolo Serena, *Senior Member, IEEE*, Chiara Lasagni, *Member, IEEE*, Alberto Bononi, *Senior Member, IEEE*, Fabien Boitier, *Member, IEEE*, and Joana Girard-Jollet

Abstract—We propose a block least mean square (LMS) algorithm to monitor the longitudinal power profile of a fiber-optic link through receiver-based digital data from a coherent detector. Compared to the benchmark least squares (LS) method, the proposed algorithm does not require large matrix inversions or batch processing, thus allowing the received data to be processed in blocks of minimum size by an overlap-save algorithm, reducing complexity and latency. We propose an efficient implementation of the method with a stochastic gradient update leveraging a key computation in the frequency domain, offering computational savings over state-of-the-art monitoring techniques. We test the proposal in different scenarios by means of numerical simulations.

Index Terms—Least mean square (LMS), longitudinal power profile monitoring, overlap-save

I. INTRODUCTION

DIGITAL longitudinal monitoring techniques have received a lot of interest in recent years because they open up new possibilities in autonomous network control through post-processing inference rather than by distributed intrusive optical hardware devices [1]. The core objective is to leverage received data from a digital receiver to perform system identification, thereby offering the possibility to reduce the interaction with a control plane. This attribute is especially important in modern optical systems that operate in disaggregated network environments provided by several suppliers and links comprising diverse optical fibers.

Longitudinal power profile estimation (PPE) is one of the most important monitoring techniques, because the primary cause of performance degradation is typically due to anomalous losses that occur during field propagation [2], [3]. Such kind of anomalies induce soft failures, which result in a gradual degradation of quality of transmission (QoT) that does not immediately cause a complete service outage. A quick and

reliable understanding of them is critical in order to implement proactive countermeasures before a soft failure turns into a hard failure.

After the introduction of coherent detection in optical communication products, the use of coherent receiver's data for monitoring linear dispersive impairments such as group velocity dispersion (GVD), polarization mode dispersion (PMD), and polarization dependent loss (PDL) captured the attention of the community, see e.g., [4]. Tanimura et al. [2], [5] were among the first to exploit the nonlinear interference (NLI) caused by the fiber Kerr effect for tackling the PPE problem. They were able to perform PPE using a correlation measurement (CM) between the coherent detector real system output and a digital twin output. Such a study revealed the relevance of describing the digital twin using a perturbative approximation [6] with an NLI that is linearly related to the power profile. This research prompted a thorough investigation and inspired innovative solutions to its core challenges [7]–[20]. A fundamental result has been provided by Sasai et al. [3], who showed that the PPE problem can be efficiently addressed using a least squares (LS) technique, a standard approach for linear system identification. Contrary to the CM method, the LS method does not need a calibration stage and thereby inherently eliminates any systematic bias. Moreover, it improves the spatial resolution compared to CM [21].

Although the least squares technique is one of the most efficient in linear adaptive filter theory in terms of convergence speed, it is complex since it requires the manipulation of a large matrix—particularly the computation of its inverse—and must be implemented within a resource-intensive digital twin architecture. Furthermore, it uses batch processing to handle the full dataset without adaptivity in its fundamental form. For these reasons, processing short blocks of data is desirable in a real-world setting because it reduces processing cost while successfully tracking a time-varying environment at reduced latency. Solutions to overcome the least squares issues exist, such as the recursive least squares (RLS) algorithm [22] or averaging several batches of data. However, the first is even more complex, while the second may introduce some artifacts [23]. The problem of complexity is particularly challenging and may prevent the implementation of the PPE inside a transceiver digital signal processor (DSP), with a peripheral field-programmable gate array (FPGA) or even a power-hungry computer being the preferred solution [24]. To mitigate the complexity of the digital twin, researchers have explored the application of machine learning techniques (see [1] and the references therein). However, the effectiveness of these

Manuscript received ***** **, 2026. This work has been supported by University of Parma through the action *Bando di Ateneo 2023 per la ricerca*.

P. Serena, C. Lasagni, and A. Bononi are with the Department of Engineering and Architecture, Università degli Studi di Parma, Parma, 43124, Italy, and with the CNIT national laboratory of advanced optical fibers for photonics (FIBERS) (e-mail: paolo.serena@unipr.it; chiara.lasagni@unipr.it; alberto.bononi@unipr.it). F. Boitier and J. Girard-Jollet are with Nokia Bell Labs, Massy, 91300, France (e-mail: fabien.boitier@nokia-bell-labs.com; joana.girard_jollet@nokia.com).

This work has been submitted to the IEEE for possible publication. Copyright may be transferred without notice, after which this version may no longer be accessible.

Color versions of one or more of the figures in this paper are available online at <http://xxxxxxxxxx.xxx.xxx>.

Digital Object Identifier xx.xxxx/JLT.xxxx.xxxxxx

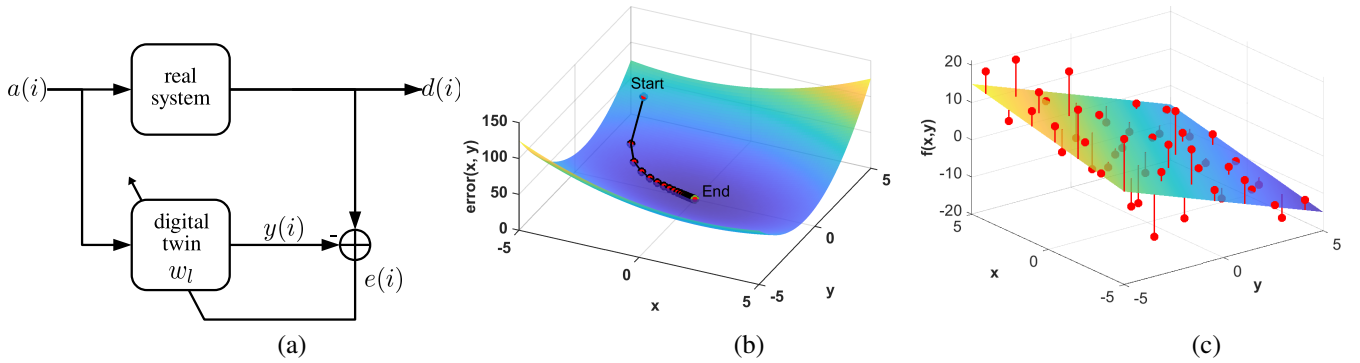


Fig. 1. (a): system identification problem setup. The objective is to find the adaptive taps w_l of the digital twin that minimize the error e between its output y and the desired output d in the presence of noise. (b): LMS concept based on a stochastic gradient update using the most recent observables. (c): Least squares method where all observables (red dots) are used to fit the desired function, here a plane.

approaches is often limited in operational networks, both because of the huge dataset required to track a dynamic network evolution, and also because of lack of measurements [25], since soft failures, which are essential for training the models, occur only rarely in highly reliable optical systems.

The least mean squares (LMS) approach is arguably the most widely-used algorithm in adaptive filter theory [22]. The reason is related to its inherent simplicity, since the LMS completely avoids the large matrix and batch processing problems associated with the standard LS technique. Since the PPE problem in a perturbative framework is linear, in this work we fill a gap in the literature by adapting the LMS algorithm to the PPE scenario. The implementation is not straightforward, because GVD may impose significant memory requirements inside the digital twin, for which efficient solutions exist provided to work with block processing rather than with the sample-by-sample processing of the standard LMS. Consequently, we use a block LMS approach, which provides a trade off between the basic LMS and the LS algorithms. However, we cannot directly adopt the block LMS theory since we face a mixed space-time problem that is not analyzed in standard LMS theory [22]. Our technique computes the stochastic gradient by using a key connection between the frequency and time domains, allowing for efficient fast Fourier transforms (FFTs) while limiting block processing to the minimum size dictated by the link's GVD.

The remainder of the paper is organized as follows. Section II discusses the system identification problem and the differences between the analog twin and the digital twin we use. Section III describes the proposed block LMS algorithm. Section IV shows the numerical results of the algorithm in different scenarios. Finally, in Section V we draw our main conclusions.

II. PROBLEM STATEMENT

The power profile estimation is a system identification problem that can be generally represented as shown in Fig. 1 (a). If we have a digital twin that accurately replicates the core behavior of the real system as much as possible, we have discovered the unknown power profile of the link under investigation. In this work, we concentrate on replicating the

propagation in the optical fibers, reserving the analysis of other devices for future studies.

Sasai et al. [3] used a perturbative approximation of the non-linear link [6], [26] to make the identification problem linear, and solved it with a LS technique which is widely regarded as one of the most accurate methods for linear systems. In this work we focus on the other popular algorithm, the LMS, and adapt it to the peculiar properties of the NLI. A comparison between the two methods is sketched in Fig. 1 (b–c). The LMS aims at minimizing an error signal iteratively by a sequence of steps using a stochastic gradient approximation calculated on the most recent data, like searching for a valley in the fog. The LS method, on the other hand, attempts to fit a parametric function to the real system response by minimizing the mean square error between them. Thus the key difference is that the LMS, in its basic form, operates sample-by-sample, while the least squares operates via batch processing. In this work we used a block-LMS technique to slightly relax the sample-by-sample feature in favor of fast convolutions through FFT. Before introducing it, we discuss the relation between a digital twin and a standard analog twin.

A. Analog twin

Given the transmitted electric field $A(t)$, a reasonable approximation of the received field using a first-order regular perturbation (RP) approximation is:

$$A_{\text{out}}(t) \approx A(t) + n_{\text{SPM}}(t) + r(t) \quad (1)$$

with n_{SPM} the NLI caused by self-phase modulation (SPM) and $r(t)$ the remaining noise, such as amplified spontaneous emission (ASE) and cross-channel NLI. According to the RP method [6], the NLI is the result of a linear accumulation along the distance:

$$n_{\text{SPM}}(t) = -j \int \gamma'(z) u(z, t) dz \quad (2)$$

where, as in [3], we introduced $\gamma'(z) \triangleq \gamma(z)f(z)$, with $\gamma(z)$ the fiber nonlinear coefficient, $f(z)$ the longitudinal optical power profile, and

$$u(z, t) \triangleq (g_z \otimes \mathcal{N}(h_z \otimes A))(t). \quad (3)$$

In this formulation, the symbol \otimes indicates temporal convolution, whereas $\mathcal{N}(A) \triangleq \|A\|^2 A$ is the nonlinear Kerr operator with $\|\cdot\|$ indicating the Euclidean norm. The symbol $h_z(t)$ is the impulse response of GVD from system input to link coordinate z , while $g_z(t)$ is the impulse response of GVD from z to system end.

Even at typical powers, the approximation (1) could be inadequate because the nonlinear Kerr effect manifests itself not only as an additive term but also as a phase that may be far from zero radians, thus weakening the Taylor approximation at the core of the RP method. The enhanced RP (eRP) [6], which makes the transformation

$$A_{\text{out}}(t) = e^{j\varphi} E(t)$$

offers a better approximation by perturbing E only:

$$A_{\text{out}}(t) \approx e^{j\varphi} (A(t) + n_{\text{SPM}}(t) - j\varphi A(t)) + r(t).$$

While the term $\exp(j\varphi)$ is irrelevant to our discussion because it is eliminated by the carrier phase recovery, the “eRP correction” given by $j\varphi A$ is crucial [21].

A reasonable choice for φ is the time average phase rotation induced by the Kerr effect [26], [27]. However, since the eRP correction is linear in φ , we found it more convenient to allow the LMS finding its best approximation for φ . This idea generalizes the proposal of [28] within the scope of the RP approach, and decreases the algorithm’s dependency on prior information.

B. Digital twin

At the optical level, the RP field (3) consists of “linear + nonlinear + linear” steps, with a GVD operator modeling each linear step separately. However, because our algorithm must work at the digital level, we actually need an RP approximation relating the transmitted/detected digital symbols rather than the input/output analog field. The fully digital twin starts with the observation that the transmitted signal is usually linearly modulated with a symbol period T by $A(t) = \sum_i a(i)p(t - iT)$, which in Fourier domain is:

$$\tilde{A}(\omega) = \tilde{a}(e^{j\omega T}) \tilde{P}(\omega) \quad (4)$$

with $\tilde{a}(e^{j\omega T})$ the discrete-time Fourier transform (DTFT) of the discrete symbol sequence $a(i)$, whereas $\tilde{A}(\omega)$ and $\tilde{P}(\omega)$ represent the Fourier transforms of $A(t)$ and $p(t)$, respectively. In this framework, $\tilde{P}(\omega)$ is an additional linear operation preceding the mentioned steps. Similarly, matched filtering and GVD equalization are extra linear operations that occur after those steps. Notably, the matched filter has frequency response that is the conjugate of the pulse’s spectrum, $\tilde{P}^*(\omega)$, and the GVD equalization similarly acts as a filter with conjugated frequency response of the GVD response. This observation enables a relationship between the impulse responses of g_z and h_z once including pulse shaping and detection in the aforementioned steps [29]:

$$\tilde{g}_z(\omega) = \tilde{h}_z^*(\omega) = \tilde{P}(\omega) e^{-j\frac{\omega^2}{2} \int_0^z \beta_2(\xi) d\xi} \quad (5)$$

with β_2 the local dispersion coefficient of the fiber. Since g_z is sufficiently band- and time-limited, we can obtain a practical

representation in the frequency domain by sampling $p(t)$ in time with N_t samples per symbol, and work with its discrete Fourier transform (DFT), while upsampling $a(i)$ to have a signal over the same temporal grid before taking its DFT. Equation (4) thus discretizes into:

$$\text{DFT} \left[A \left(\frac{mT}{N_t} \right) \right] = \text{DFT} [a_{\uparrow N_t}(m)] \times \text{DFT} \left[p \left(\frac{mT}{N_t} \right) \right]$$

with m the sample index and $\uparrow N_t$ indicating up-sampling by a factor N_t . We also need to discretize the spatial coordinate z in (2). This can be accomplished using quadrature formulas for numerical integration:

$$n_{\text{SPM}}(t) \approx \sum_l \rho_l \gamma'(z_l) u(z_l, t) \quad (6)$$

where z_l are the coordinates reproduced by the digital twin. Typically, the grid is uniform, for which a good quadrature rule is the mid-point rule¹ with ρ_l independent of l , i.e., the constant step-size.

In this framework, the digital twin builds the following signal at symbol index i :

$$y(i) = \hat{a}(i)(1 - j\varphi) + n(i) \quad (7)$$

where we identify $\hat{a}(i)$ as the detected symbols after the receiver DSP, φ as the eRP correction, and the NLI due to SPM:

$$n(i) \triangleq \sum_{l=0}^{M-1} \rho_l \gamma'(z_l) (g_l \otimes \mathcal{N}(h_l \otimes A)) (iT) \quad (8)$$

where M is the number of integration points and we introduced $h_l \equiv h_{z_l}(t)$, $g_l \equiv g_{z_l}(t)$ to simplify the notation. In the next section, we propose an efficient implementation that exploits the overlap-save algorithm within the context of our block LMS solution.

III. BLOCK LMS BASED ON OVERLAP-SAVE

System identification is generally accomplished by minimizing an error function. Since the problem is stochastic, ensemble averaging of the error function is commonly utilized in analytical works because it is simple to manipulate in linear systems, as demonstrated by Wiener in his seminal works [22]. Unfortunately, using ensemble averaging is impractical in many problems, including the one we seek to solve, because it requires the observation of many independent realizations of the system. The common solution is to replace ensemble averaging with deterministic averaging, which results in the least squares method. LMS reduces deterministic averaging to its most basic form, namely taking the current realization of the error. This simple approximation has significant implications because it reduces the complexity and allows for a recursive search for the minimum by a stochastic gradient method, thus by recursively updating the result by taking short steps in the steepest descent direction, see Fig. 1(b).

According to the previous Section, the input/output relation of the optical link is linear in the longitudinal power profile

¹We recall that the mid-point rule is more accurate than the more common trapezoidal rule without adding complexity.

and more generally in the $\gamma'(z_l)$ coefficients. We collect such coefficients into a vector of length M

$$\mathbf{w}(i) = [\gamma'(z_0), \gamma'(z_1), \dots, \gamma'(z_{M-1})]^T$$

and introduce a temporal dependence on the symbol i . The steepest descent updating rule is [22]:

$$\mathbf{w}(i+1) = \mathbf{w}(i) - \frac{\mu}{2} \nabla J(i)$$

where J is the error function that we want to minimize and the gradient ∇ is with respect to the taps \mathbf{w} . According to Fig 1(a), the error is $e(i) = d(i) - y(i)$, with $d(i)$ the desired response at time i (the real system output) and $y(i)$ the corresponding digital twin output. The steepest descent method uses $J = \mathbb{E}[|e(i)|^2]$ while the LMS simply $J = |e(i)|^2$. Unfortunately, the basic LMS rule works on a sample-by-sample basis, preventing the use of efficient techniques like the FFT that operate over blocks of data. However, the use of FFT is particularly desirable because the NLI involves convolutions with filters that may have a long duration. A block-LMS appears to be the most logical solution to this problem. The idea is to update the taps not at each sample but at each block of samples (mini batch), chosen longer than the system memory, so that FFTs can be utilized. Nevertheless, the error function J varies across the block, hence it has been recommended to use averaging to get a unique value [22, chap. 8]. Using k to indicate block index, we thus use the following updating rule:

$$\mathbf{w}(k+1) = \mathbf{w}(k) - \frac{\mu}{2} \sum_{i=0}^{L-1} \nabla J(kL+i) \quad (9)$$

where each block contains L symbols. A significant distinction exists between our proposed block LMS and the conventional block LMS [22]: the former addresses a mixed space-time problem that is time-invariant but space-variant with respect to the key variable under investigation. Our goal is to leverage the time-invariant property for efficient operations by expressing both the digital twin output y and the tap update rule with optimized computational methods.

We begin our analysis with y . Thanks to the overlap-save algorithm (see (12)), we have the following relation between the analog signal (3) and its discrete counterpart for $i = 0, 1, \dots, L-1$:

$$(g_l \otimes \mathcal{N}(h_l \otimes A))((kL+i)T) = \left(g_{l,\text{pad}} \otimes \mathcal{N}(h_{l,\text{pad}} \otimes \hat{A}_k) \right)_{\text{val}}(iN_t)$$

where we converted an analog problem based on linear convolutions \otimes into a discrete one using efficient circular convolutions \circledast . While we refer the reader to Appendix A for more details, \hat{A}_k is a vector resulting from the concatenation of the symbols in block $(k-1)$ and block k , subsequently upsampled by a factor N_t . “val” refers the not-aliased part of the vector, while “pad” means zero-padded. All vectors are of length $(2L \times N_t)$, where the factor two is consistent with the block concatenation. Additionally, we observe that we are employing multirate DSP, with increased sampling frequency

to handle optical fields and downsampling by a factor of N_t for the final output.

To simplify the notation, we introduce a vector containing aliased and non-aliased samples:

$$U_{lk} \triangleq \left(g_{l,\text{pad}} \otimes \mathcal{N}(h_{l,\text{pad}} \otimes \hat{A}_k) \right)(n), \quad n = 0, \dots, 2LN_t-1$$

and exploit the properties of the DFT to transform (8) into:

$$n(i) = \left(\text{DFT}^{-1} \left[\sum_{l=0}^{M-1} \rho_l w_l(k) \cdot \text{DFT}[U_{lk}] \right] \right)_{\text{val}}(iN_t), \quad i = 0, \dots, L-1$$

where w_l is the l th element of \mathbf{w} . Note that we return back to the time domain only after having computed the summation in l , thus with only one final IFFT. Finally, the computation of $y(m)$ follows straightforwardly from (7).

Regarding the tap-update rule, the LMS transforms (9) into [22]:

$$\mathbf{w}(k+1) = \mathbf{w}(k) + \mu \text{Re}[\mathbf{v}(k)] \quad (10)$$

where \mathbf{v} is an $M \times 1$ vector whose j th element $v_j(k)$ is:

$$\begin{aligned} v_j(k) &= \sum_{i=0}^{L-1} e_k^*(i) (g_j \otimes \mathcal{N}(h_j \otimes A_k))(iT) \\ &= \sum_{i=0}^{L-1} e_k^*(i) (U_{jk})_{\text{val}}(iN_t) \\ &= \sum_{n=0}^{2LN_t-1} e_{k,\text{int}}^*(n) U_{jk}(n) \\ &= \frac{1}{2LN_t} \sum_{f=0}^{2LN_t-1} \tilde{e}_{k,\text{int}}^*(f) \tilde{U}_{jk}(f), \quad j = 0, 1, \dots, M-1 \end{aligned}$$

where $e_k(i) \triangleq e(kL+i)$ is the error in block k , tilde indicates DFT, and we used the Parseval's theorem [30] in the last identity, which is crucial for an efficient implementation. $e_{k,\text{int}}$ is a vector resulting from upsampling $e_k(i)$ by a factor N_t and subsequently applying zero-padding specifically at the indexes where U_{jk} contains non-valid samples, allowing us to process the full U_{jk} vector rather than the subset $(U_{jk})_{\text{val}}$ and thus the use of Parseval's theorem. This approach allows the computation of $g_j \otimes \mathcal{N}(h_j \otimes A_k)$ in the frequency domain in the local k th window, thereby saving M IFFT at the cost of one extra FFT for $e_{k,\text{int}}$.

We found it useful to update the eRP correction φ independently of the taps \mathbf{w} , with a new control on its step size, called μ_0 . Hence we treat it as an independent finite impulse response (FIR) filter with one tap, φ , whose update rule follows similarly:

$$\varphi(k+1) = \varphi(k) + \mu_0 \text{Im} \left[\sum_{i=0}^{L-1} e_k^*(i) \hat{a}(kL+i) \right] \quad (11)$$

where the imaginary part is strictly related to the j in front of φ in (7).

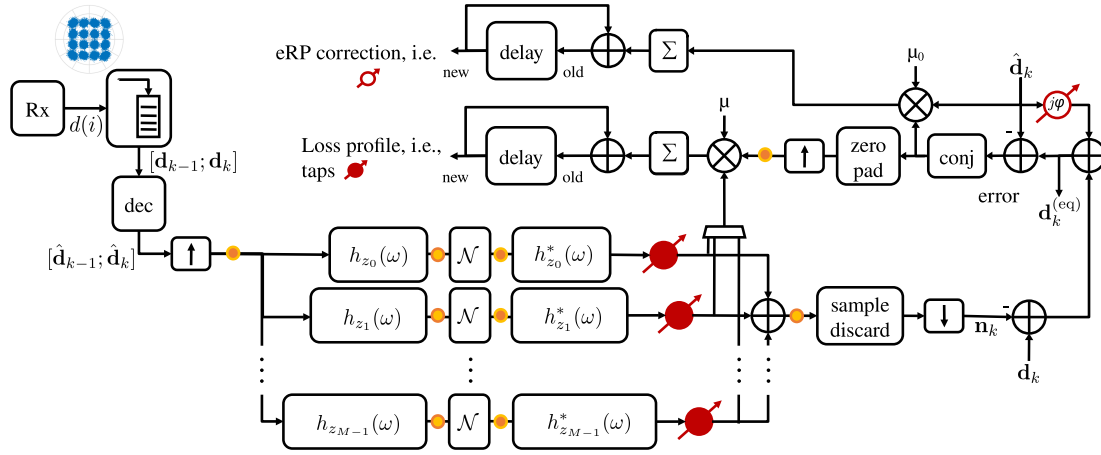


Fig. 2. LMS block diagram for monitoring the longitudinal power profile (represented by the filled taps) at coordinates z_l . The dark circle with a light ring represents FFT, while inverted colors indicate IFFT. An equalized replica of the data, $\mathbf{d}_k^{(eq)}$, is a concomitant outcome of the monitoring procedure.

A. Block diagram

A block diagram of the proposed LMS power profile monitor is shown in Fig. 2. The Rx block at the top-left corner outputs the received noisy symbols from a typical receiver-DSP including matched filtering, equalization, time recovery, frequency and carrier phase recovery. The Rx symbols are then buffered into vectors

$$\mathbf{d}_k \triangleq [d(kL), \dots, d(kL + L)]^T$$

describing the blocks. These blocks are then concatenated in pairs, i.e., $[\mathbf{d}_{k-1}; \mathbf{d}_k]$, as per the overlap-save idea. The block length L must exceed the duration of the system memory, which is set by GVD and the matched filter duration. As a rule of thumb, the memory that GVD adds in a fiber of length z is $2\pi|\beta_2|z/T^2$ symbols.

The module “dec” corresponds to decision and potentially includes forward-error correction, provided that its challenges, in particular latency, can be addressed [31]–[33]. Then, the signal is upsampled to create the vector \hat{A}_k . We used upsampling of $N_t = 2$ samples per symbol, which is enough to capture the pulse bandwidth. It is worth noting that aliasing occurs within the nonlinear block when the pulse roll-off is greater than zero. However, our results with roll-off of 0.1 did not show any significant aliasing.

After upsampling we use FFT to move into the frequency domain, which is shown as a dark orange circle with a light yellow ring for notation purposes (and an inverted scheme for IFFT). The corresponding DFT is then propagated into the digital twin through a sequence of parallel “linear+nonlinear+linear” steps at the heart of the RP approximation, as explained in Section II-B. Each local contribution is then weighted by the corresponding tap w_l , which is the primary objective of our algorithm. Note that we return back to the time domain by an IFFT only after summing all the NLI contributions in the frequency domain, thus significantly saving on FFT operations. This is possible because we calculate the error function that drives the LMS in the frequency domain. Similarly, we performed a single FFT of \hat{A}_k at the

beginning, thus limiting the computational effort to one FFT and one IFFT per path.

After returning to the time domain, the aliased samples from the overlap-save algorithm are discarded (operation indicated by “val” in our analysis), and the signal is then downsampled back to one sample per symbol. We thus have an estimation of the NLI (8) within the k th block of symbols, indicated by \mathbf{n}_k . We then remove the SPM-NLI and the eRP correction from the received noisy symbols to obtain the cleaner signal $\mathbf{d}_k^{(eq)}$, as we have effectively created a spatially resolved Volterra nonlinear equalizer that functions alongside the monitoring device. Finally, we calculate the error $e(i) = d(i) - y(i)$ for each index i in the block and update the taps of the eRP correction and of the γ' coefficients block-by-block as described in the previous Section. Note that the last operation exploits a frequency domain computation after zero-padding and summation thanks to Parseval’s theorem.

Even though the block diagram refers to a single signal, with dual polarization we just duplicate the operations. However, if PMD and PDL are small, we recommend leveraging the correlated NLI in the two polarizations by averaging their error functions to mitigate the noise.

B. Polyphase implementation

The upsampler and downsampler can be removed when using a polyphase implementation with additional parallelization [30]. Figure 3 illustrates the equivalence between a single branch of the digital twin and its polyphase structure using $N_t = 2$. The impulse responses $h'_z(i)$ and $h''_z(i)$ contain the odd and even samples of $h_z(i)$, respectively. The main advantage of a polyphase representation is a reduced sampling rate (one sample per symbol) achieved by using smaller, parallel filters instead of one large filter. When using the polyphase structure, we can also remove the extra upsampler of the error signal in Fig. 2, thus applying Parseval’s theorem on the DFT of a signal sampled at one sample per symbol.

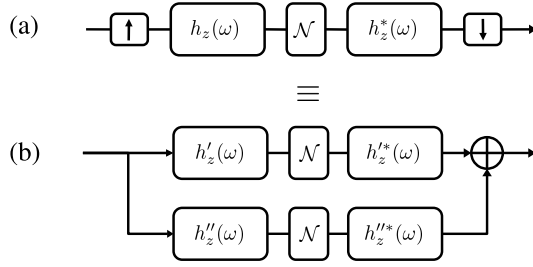


Fig. 3. (a) One branch of the block diagram shown in Fig. 2. (b) Polyphase implementation of the branch. The two structures are equivalent with similar complexity; however the polyphase one works at a halved sampling rate.

IV. NUMERICAL RESULTS

We tested the proposed LMS algorithm on a dual-polarization 16 quadrature amplitude modulated (QAM) channel at 64 Gbd. The “real system” was modeled by a numerical simulation with the split-step Fourier method (SSFM), by launching sequences of 65536 symbols shaped with root-raised-cosine pulses of roll-off 0.1 into an optical link with 100-km spans and lumped amplification. The SSFM step was updated with the constant local error (CLE) criterion [34] with a first step of 200 m. The optical fibers had nominal loss coefficient of 0.2 dB/km, dispersion $17 \text{ ps} \cdot \text{nm}^{-1} \text{km}^{-1}$, nonlinear coefficient $\gamma = 1.26 \text{ W}^{-1} \text{km}^{-1}$. PMD and PDL were absent. We assumed the LMS to have perfect knowledge of the fiber dispersion and of the Tx symbols (except one result). To test the monitoring capabilities, we inserted one or multiple lumped loss anomalies at different positions of the link depending on the setup. Since ASE and cross-channel Kerr effects act as noise for the algorithm, we simulated them through receiver noise loading of an additive white Gaussian noise (AWGN) source, $r(t)$ in our analysis, with the signal-to-noise ratio (SNR) as a control variable. We used a basic matched-filter receiver with GVD and average carrier phase recovery.

We started by testing the algorithm in the absence of noise to test its capabilities. We analyzed a multi-anomaly case in a single span, including: i) six loss anomalies of 0.25 dB each, and ii) backward Raman amplification. Signal power was $P = 5 \text{ dBm}$, while we iterated the LMS over 1000 independent realizations of the real system. In (9) we used $\mu = \bar{\mu}/P^{5/2}$ with $\bar{\mu} = 0.05$, where the normalization to $P^{5/2}$ is an attempt to establish a general rule of thumb. The scaling was motivated by a predicted scaling with P^3 of the NLI variance [26] and a scaling with P^2 of the error variance on the (normalized) constellation. On the other hand, in (11) we used $\mu_0 = 2 \cdot 10^{-4} \Phi$ with Φ the average nonlinear phase accumulated in the link. The spatial resolution of the digital twin was 5 km.

Figure 4 shows the true loss profile and the predicted one by the LMS algorithm. The match is excellent, with a slight overestimation in the low power regime, a problem common to any NLI-based technique where the useful signal is soaked in noise.

Like any LMS method, the normalized step size $\bar{\mu}$ is a trade off between speed of convergence and accuracy. To test such trade-off, we analyzed a three-span link with anomaly

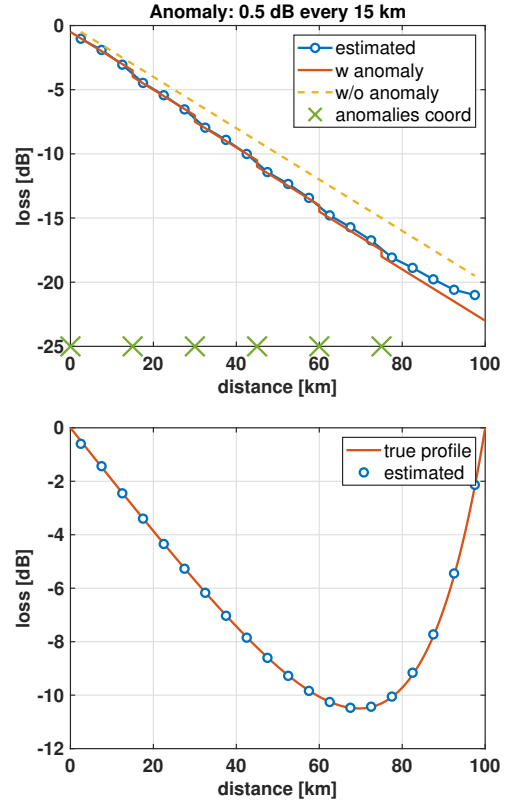


Fig. 4. Top: A multianomaly case with six loss anomalies of 0.25 dB every 15 km. Bottom: net loss profile in the presence of backward Raman pumping. No additive noise.

of 1 dB after 125 km, hence roughly after one effective length in the second span. In this simulation we employed an exceptionally low SNR of 10 dB to stress the behavior under an extreme situation. For reference, a 16-QAM signal in an AWGN channel at SNR=10 dB has at best a mutual information of 3.27 bits/symbol, smaller than its 4 bits/symbol nominal value, thus requiring a forward error correction (FEC) redundancy of at least 0.73 bits/symbol. As a quality metric, we estimated the root mean square error (RMSE) between the estimated profile and the true one in dB scale. As observed previously, since perturbative methods fail in the low power regions, we decided to reject results at coordinates with a path loss greater than 15 dB. This ensures that excess errors do not undermine the meaning of the RMSE.

The RMSE is shown in Fig. 5. To provide context for the RMSE, keep in mind that knowledge of only the nominal loss profile excluding anomalies yields an RMSE in this setup of 0.5 dB. We observe an improvement over this benchmark, with the RMSE eventually decreasing as the number of samples increases. The estimation becomes unstable at $\bar{\mu} = 0.2$, even though it is able to converge reasonably well. It is worth mentioning that while any starting value for the filter taps is feasible, different initial setups will result in different convergence rates and paths. In our simulations, we initialized the taps with knowledge of the nominal fiber loss, which allowed for faster convergence than a random or zero-initialized start.

To test the performance against a single loss anomaly value

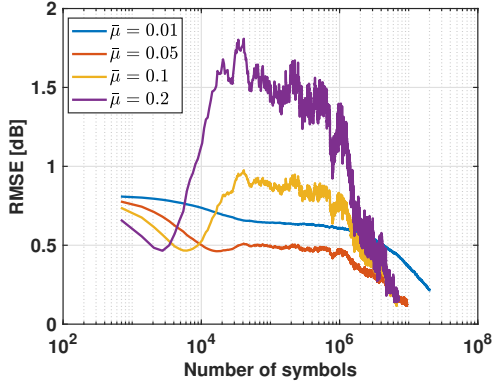


Fig. 5. RMSE vs. the number of symbols processed by the LMS algorithm at different normalized LMS step sizes $\bar{\mu}$. Three-span link with anomaly of 1 dB after 125 km. Taps initialized with the nominal fiber loss.

or its position, we varied them in the previous three-span system. Figure 6 depicts the results in terms of the RMS error, which is still restricted to losses smaller than 15 dB. We observe an excellent behavior with respect to both variables, with minor impact of the SNR in the selected ranges.

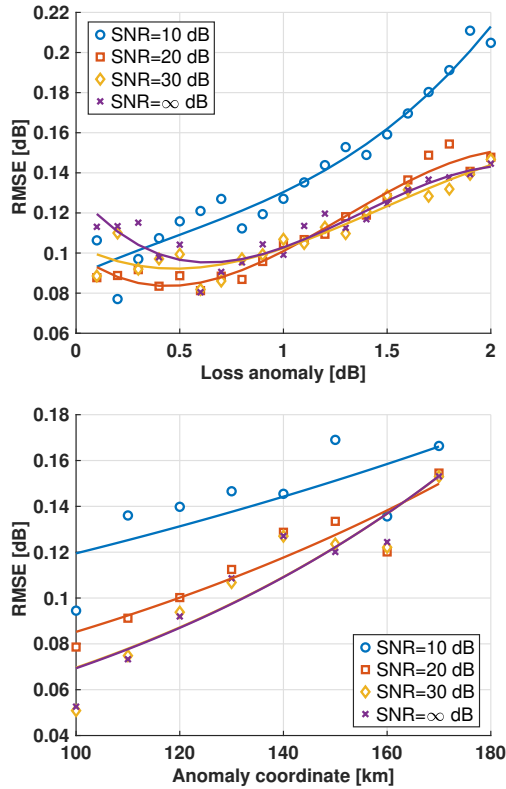


Fig. 6. RMSE in the three-span system. Top: single loss anomaly of variable magnitude located at 125 km. Bottom: loss anomaly of 1 dB at a variable location. The lines are interpolations to guide the eye.

Next we tested the impact of the signal power. Figure 7 illustrates the algorithm behavior, both in terms of the RMSE and SPM compensation capabilities. Here we used SNR=20 dB. The primary performance metric, the RMSE, is shown on the left y-axis. We observe a failure of the method at

very low power, where the residual noise dominates the NLI power due to SPM. However, it is worth noting that the algorithm is capable of detecting the useful signal, SPM, even if the SNR associated to the residual noise is smaller than the SNR associated to SPM, as visible in the right-axis. We also reported for comparison the SNR of SPM after nonlinear equalization, hence by computing the noise power on the residual NLI of $\mathbf{d}_k^{(eq)}$. We observe a significant reduction of SPM with the chosen grid of 5 km, highlighting the potential for SPM compensation performed together with monitoring.

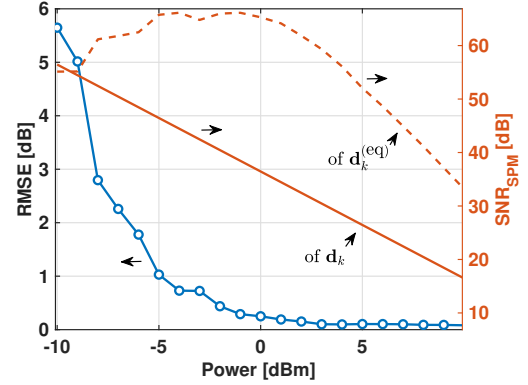


Fig. 7. (Left) RMSE vs. signal power with a residual noise SNR of 20 dB. (Right) SNR associated with SPM only experienced by the detected symbols \mathbf{d}_k or equalized symbols $\mathbf{d}_k^{(eq)}$. The results are for a three-span link

In another test we investigated the impact of the spatial grid used in the digital twin, see (6). We estimated the RMS error vs the number of steps per span in the three-span system, here at SNR=10 dB. The result is shown in Fig. 8, which we remind is based on a mid-point numerical integration rule. The anomaly was at 125 km. Clearly, we see a decline in performance with fewer steps per span. The explanation is related to the the digital twin's inability to reproduce the real system. Therefore, if computational complexity is a concern, it may be beneficial to explore more efficient quadrature rules for numerical integration. As a rough estimate, we observe a severe degradation of performance around ≈ 14 steps per span (step size ≈ 7 km), corresponding to a phase shift of GVD in the frequency domain of π at the signal 3dB bandwidth.

Having tested the algorithm in terrestrial links, we then moved to a subsea link. We examined a transatlantic 86-span with 70 km per span (total 6020 km), with two loss anomalies of 1 dB at zero and 5950 km, i.e., at the beginning of the first and the last span. We changed the link parameters to suit the different scenario, hence we used dispersion $21 \text{ ps}\cdot\text{nm}^{-1}\text{km}^{-1}$, nominal loss 0.155 dB/km , $\gamma = 0.92 \text{ W}^{-1}\text{km}^{-1}$, and channel power -1 dBm . The SNR was 10 dB, a realistic number for such a system. Figure 9 shows the loss profile estimated with the LMS after 32M symbols and the true one, observing an excellent match. It is worth noting that in this ultralong case we had to reduce $\bar{\mu}$ to 0.01. In the subsea case, the computational effort is significant because both the GVD memory, thus the block size L , and the spatial grid size grow linearly with distance.

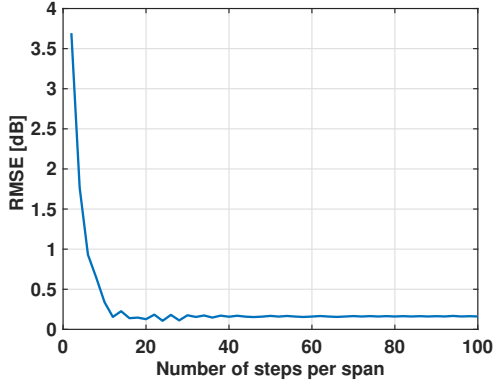


Fig. 8. RMSE vs the number of steps per span adopted in the digital twin. The results are for a three-span link with a residual noise SNR of 10 dB.

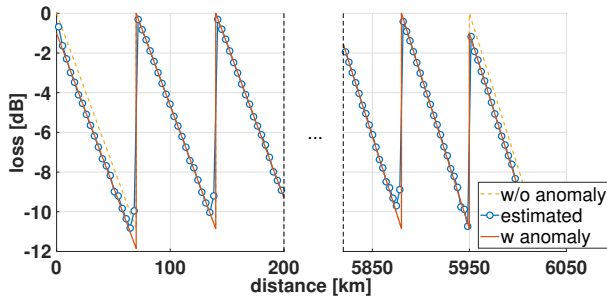


Fig. 9. Subsea link of 6020 km with two loss anomalies at the beginning of the first and the last span, respectively. SNR=10 dB.

The previous results were in data-aided mode. To check the impact of wrong decisions we tested the behavior by feeding the digital twin with the pre-FEC decided data. As a quality factor, we evaluated the RMSE versus symbol error rate (SER), as shown in Fig. 10. The SER was controlled by varying the residual noise SNR. Here we analyzed a 10×100 km link with a loss anomaly placed at various positions, z_{an} in the figure. The results show that algorithm performance worsens as SER increases, regardless of the position of the anomaly, with a maximum tolerable SER of around 10^{-3} . We thus deduce that longer connections suffer more from this requirement.

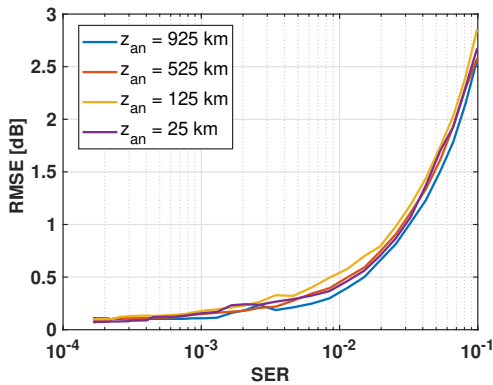


Fig. 10. RMSE vs symbol error rate. Decision-directed LMS without FEC. Loss anomaly of 1 dB at different positions (z_{an}) of a 10×100 km link.

V. CONCLUSIONS

We proposed a block LMS technique for monitoring the longitudinal power profile of a fiber-optic link. The proposed technique is efficient, based on a full digital twin of the link, and is adaptive by nature, using a stochastic gradient descent updating rule based on a technique in the frequency domain. We process data by using an overlap-save algorithm, avoiding the need for batch processing of large datasets. The proposed method leverages the main advantages of the LMS algorithm in the context of linear adaptive filter theory, like its simplicity and small memory footprint. Compared with the least squares method, there is no need to invert a large matrix. The proposed method is able to identify multiple loss anomalies without the need of a calibration stage.

In its current version, the algorithm just requires knowledge of fiber dispersion. Future research will focus on expanding the digital twin to include more complex optical devices.

APPENDIX A OVERLAP-SAVE ALGORITHM

In this appendix we review the basic properties of the overlap-save algorithm [22], [30] and specialize them to our framework. Let $y(i)$ be the output of the linear discrete convolution \otimes between a FIR filter of L samples and a longer signal x :

$$y(i) = (h \otimes x)(i) = \sum_n h(n)x(i-n).$$

The overlap-save algorithm is an efficient method to compute $y(kL+i)$ for a given integer k and $i = 0, \dots, L-1$, i.e., to compute y within the k th block of L samples. The key relationship at the hearth of the method is:

$$(h \otimes x)(kL+i) \equiv (h_{\text{pad}} \circledast x_k)_{\text{val}}(i), \quad i = 0, \dots, L-1 \quad (12)$$

where \circledast indicates circular convolution, x_k is a vector of $2L$ samples resulting from the concatenation of the input signal in blocks $(k-1, k)$:

$$x_k \triangleq x(i), \quad i = (k-1)L, \dots, (k+1)L-1. \quad (13)$$

The subscript “val” denotes the valid, not-aliased part of the circular convolution result, which corresponds to the latter half of the output vector. However, keep in mind that a processing delay is inherent when, like in our case, the digital twin models the real system using a FIR implementation of non-causal filters. h_{pad} is:

$$h_{\text{pad}}(i) \triangleq \begin{cases} h(i) & i = 0, 1, \dots, L-1 \\ 0 & i = L, \dots, 2L-1. \end{cases} \quad (14)$$

Note that it is not necessary to split x into blocks of L samples. Longer blocks imply redundant operations, whereas shorter blocks reduce processing latency [22]. Setting the block length equal to L is generally considered as an optimal choice.

REFERENCES

- [1] D. Wang et al., "Digital Twin of Optical Networks: A Review of Recent Advances and Future Trends," *J. Lightw. Technol.*, vol. 42, no. 12, pp. 4233–4259, June 2024.
- [2] T. Tanimura, S. Yoshida, K. Tajima, S. Oda, and T. Hoshida, "Fiber longitudinal anomaly position identification over multi-span transmission link out of receiver-end signals," *J. Lightw. Technol.*, vol. 38, no. 9, pp. 2726–2733, May 2020.
- [3] T. Sasai, M. Takahashi, M. Nakamura, E. Yamazaki, and Y. Kisaka, "Linear Least Squares Estimation of Fiber-Longitudinal Optical Power Profile," *J. Lightw. Technol.*, vol. 42, no. 6, pp. 1955–1965, Mar. 2024.
- [4] F. N. Hauske, M. Kuschnerov, B. Spinnler, and B. Lankl, "Optical Performance Monitoring in Digital Coherent Receivers," *J. Lightw. Technol.*, vol. 27, no. 16, pp. 3623–3631, Aug. 2009.
- [5] T. Tanimura, T. Hoshida, Y. Hanamaki, H. Nakashima, K. Hama, T. Tanaka, H. Onaka, J. C. Rasmussen, e H. Yamauchi, "Semi-blind nonlinear equalization in coherent multi-span transmission system with inhomogeneous span parameters," in Proc. *Opt. Fiber Commun. Conf. (OFC)*, San Diego, CA, USA, Mar. 2010, paper OMR6.
- [6] A. Vannucci, P. Serena, and A. Bononi, "The RP Method: A New Tool for the Iterative Solution of the Nonlinear Schrodinger Equation," *J. Lightw. Technol.*, vol. 20, no. 7, pp. 1102–1112, July 2002.
- [7] T. Sasai, M. Nakamura, E. Yamazaki, S. Yamamoto, H. Nishizawa, and Y. Kisaka, "Digital longitudinal monitoring of optical fiber communication link," *J. Lightw. Technol.*, vol. 40, no. 8, pp. 2390–2408, Apr. 2022.
- [8] S. Gleb, K. Pankratov, and J. Luo, "Fiber link anomaly detection and estimation based on signal nonlinearity," in Proc. *Eur. Conf. Opt. Commun. (ECOC)*, Bordeaux, France, Sep. 2021, paper We3B.3.
- [9] M. R. Sena, R. Emmerich, B. Shariati, C. Santos, A. Napoli, J. K. Fischer, and R. Freund, "DSP-based link tomography for amplifier gain estimation and anomaly detection in C+L-band systems," *J. Lightw. Technol.*, vol. 40, no. 11, pp. 3395–3405, June 2022.
- [10] M. Takahashi, T. Sasai, E. Yamazaki, and Y. Kisaka, "Experimental demonstration of monitoring PDL value and location using DSP-based longitudinal power estimation with linear least squares," in Proc. *Eur. Conf. Opt. Commun. (ECOC)*, Glasgow, Scotland, Oct. 2023, paper P14.
- [11] A. May, F. Boitier, E. Awwad, P. Ramantanis, M. Lonardi, and P. Ciblat, "Receiver-based experimental estimation of power losses in optical networks," *IEEE Photon. Technol. Lett.*, vol. 33, no. 22, pp. 1238–1241, Nov. 2021.
- [12] A. May, F. Boitier, A. Courilleau, B. Al Ayoubi, and P. Layec, "Demonstration of Enhanced Power Losses Characterization in Optical Networks," in Proc. *Opt. Fiber Commun. Conf. (OFC)*, San Diego, CA, USA, Mar. 2022, paper Th1C.6.
- [13] X. Zhou, R. Fan, X. Yan, and F. Zhang, "Advancing Intelligent Fiber Optic Link Monitoring: Innovations, Challenges, and Future Directions," in Proc. *Eur. Conf. Opt. Commun. (ECOC)*, Frankfurt, Germany, Sep. 2025, paper Th.01.04.3.
- [14] P. Serena, C. Lasagni, A. Bononi, F. Boitier, A. May, P. Ramantanis, and M. Lonardi, "Locating Fiber Loss Anomalies with a Receiver-side Monitoring Algorithm Exploiting Cross-phase Modulation," in Proc. *Opt. Fiber Commun. Conf. (OFC)*, San Diego, CA, USA, Mar. 2023, paper W1H.3.
- [15] R. Hui, C. Laperle, and M. O'Sullivan, "Measurement of total and longitudinal nonlinear phase shift as well as longitudinal dispersion for a fiber-optic link using a digital coherent transceiver," *J. Lightw. Technol.*, vol. 40, no. 21, pp. 7020–7029, Nov. 2022.
- [16] C. Hahn, J. Chang, and Z. Jiang, "Estimation and Localization of DGD Distributed Over Multi-Span Optical Link by Correlation Template Method," in Proc. *Opt. Fiber Commun. Conf. (OFC)*, San Diego, CA, USA, Mar. 2024, paper W1B.2.
- [17] D. Pileri, S. Straullu, A. Nespola, L. Andrenacci, S. Piciaccia, and G. Bosco, "Experimental Demonstration of Longitudinal Power Monitoring Over a Mixed Fiber Link," *IEEE Photon. Technol. Lett.*, vol. 37, no. 20, pp. 1181–1184, Oct. 2025.
- [18] A. May, F. Boitier, A. C. Meseguer, J. U. Esparza, P. Plantady, A. Calsat, and P. Layec, "Longitudinal power monitoring over a deployed 10,000-km link for submarine systems," in Proc. *Opt. Fiber Commun. Conf. (OFC)*, San Diego, CA, USA, Mar. 2023, paper Tu2G.3.
- [19] F. Boitier, A. Pacini, A. May, and P. Layec, "A Multi-Stage Method for Least-Square based Longitudinal Power Profile Computation," in Proc. *Opt. Fiber Commun. Conf. (OFC)*, San Diego, CA, USA, Mar. 2025, paper W3E.8.
- [20] T. Sasai, M. Nakamura, T. Kobayashi, H. Kawakami, E. Yamazaki, and Y. Kisaka, "Revealing Raman-amplified Power Profile and Raman Gain Spectra with Digital Backpropagation," in Proc. *Opt. Fiber Commun. Conf. (OFC)*, Washington, DC, USA, June 2021, paper M31.5.
- [21] T. Sasai, E. Yamazaki, and Y. Kisaka, "Performance limit of fiber longitudinal power profile estimation methods," *J. Lightw. Technol.*, vol. 41, no. 11, pp. 3278–3289, June 2023.
- [22] S. Haykin, *Adaptive Filter Theory*, 5th ed. International ed. Harlow, U.K.: Pearson Education, 2014.
- [23] D. Tang, Y. Jiang, and J. Luo, "Noise and Performance Analysis of Fiber-Longitudinal Power Profile Estimation," *J. Lightw. Technol.*, vol. 42, no. 17, pp. 5839–5848, Sep. 2024.
- [24] T. Tanimura, S. Yoshida, K. Tajima, S. Oda, and T. Hoshida, "Concept and implementation study of advanced DSP-based fiber-longitudinal optical power profile monitoring toward optical network tomography," *J. Opt. Commun. Netw.*, vol. 13, no. 10, pp. E132–E141, Oct. 2021.
- [25] F. Musumeci and M. Tornatore, "Failure management in optical networks with ML: a tutorial on applications, challenges, and pitfalls [Invited]," *J. Opt. Commun. Netw.*, vol. 17, no. 8, pp. C144–C155, Aug. 2025.
- [26] P. Serena and A. Bononi, "An alternative approach to the Gaussian noise model and its system implications," *J. Lightw. Technol.*, vol. 31, no. 22, pp. 3489–3499, Nov. 2013.
- [27] P. Serena and A. Bononi, "On the nonlinear reference phase in regular perturbation models," in Proc. *2015 Tyrrhenian International Workshop on Digital Communications (TIWDC)*, Florence, Italy, 2015, paper 1.1.
- [28] I. Kim, O. Vassilieva, R. Shinzaki, M. Eto, S. Oda, and P. Palacharla, "Robust Longitudinal Power Profile Estimation in Optical Networks using MMSE with Complex Scaling Factor," in Proc. *Opt. Fiber Commun. Conf. (OFC)*, San Diego, CA, USA, Mar. 2023, paper W4H.6.
- [29] A. Mecozzi and R.-J. Essiambre, "Nonlinear Shannon limit in pseudolinear coherent systems," *J. Lightw. Technol.*, vol. 30, no. 12, pp. 2011–2024, June 2012.
- [30] D. G. Manolakis and V. K. Ingle, *Applied Digital Signal Processing: Theory and Practice*. New York, NY, USA: Cambridge University Press, 2011.
- [31] J. Chang, C. Hahn, Q. Guo, and Z. Jiang, "Impact of BER on Longitudinal Power Profile Estimation and its Correction," in Proc. *Opt. Fiber Commun. Conf. (OFC)*, San Francisco, CA, USA, Mar. 2025, paper W3E.7.
- [32] L. Andrenacci, A. Nespola, S. Straullu, Y. Jiang, S. Piciaccia, G. Bosco, and D. Pileri, "Implementation Penalties for Nonlinear Interference Estimation with Linear Least Squares Longitudinal Power Monitoring," in Proc. *Opt. Fiber Commun. Conf. (OFC)*, San Francisco, CA, USA, Mar. 2025, paper W3E.5.
- [33] Y. Jiang, D. Tang, J. Luo, Y. Chen, B. Zheng, and Y. Qiao, "Mitigation of Power Offset Induced by Hard-Decision-Error in Fiber Longitudinal Power Profile Estimation," in Proc. *Opt. Fiber Commun. Conf. (OFC)*, San Francisco, CA, USA, Mar. 2025, paper W3E.6.
- [34] S. Musetti, P. Serena, and A. Bononi, "On the accuracy of split-step Fourier simulations for wideband nonlinear optical communications," *J. Lightw. Technol.*, vol. 36, no. 23, pp. 5669–5677, Dec. 2018.